ELSEVIER

Fracture Mechanics Parameters of Concrete

An Overview

Manuel Elices and Jaime Planas
Departamento de Ciencia de Materiales, Universidad Politécnica de Madrid, E.T.S.I. Caminos, Ciudad Universitaria, Madrid, Spain

The purpose of this paper is to set a scenario for discussing and comparing different models of concrete fracture. Using as a reference the cohesive crack model, as conceived by Hillerborg, it was found that simpler models—the equivalent elastic crack, the R-Δa *curve approach, or models based on two parameters such as Bazant's and Jenq-Shah's—fit inside this scheme and are hierarchically related. For each approach, the theoretical background is reviewed, the experimental aspects are discussed, and the relevance to size effect predictions is considered. This review supplies criteria for comparing the different models and provides interpretation for the measured parameters with a unified language.* ADVANCED CEMENT BASED MATERIALS 1996, 4, 116–127

KEY WORDS: Cohesive cracks, Concrete fracture, Equivalent elastic cracks, Size effect

Concrete fracture has been approached from different points of view, and literature on this subject is rich in models each claiming partial successes. Moreover, each model has its own jargon, and the reader is faced with an overwhelming amount of symbols for apparently the same concepts, as with the *fracture energy* defined in Hillerborg, Bazant, or Jenq-Shah's models, the linear elastic fracture mechanics (LEFM) approach, or, the *crack length* concept. It would be helpful to discover links between such fracture models and place them within the same framework. This will supply us with criteria for comparing the different models, and their parameters, and will help us in wandering through the increasing literature on this subject.

The reference frame chosen for comparison of the different models is based on the *cohesive crack* model. This choice is by no means the only way to compare the usual models of concrete failure, but it is widely used and flexible enough to embrace known models. Use of the cohesive model in concrete was pioneered by Hillerborg et al. [1] and since then, profitably expanded by researchers from Europe, the United States, Japan, and Australia [2–16].

This paper is structured in two main sections: First, the cohesive model, used as a reference, is reviewed. Then, the equivalent elastic crack models are discussed, with special reference to the Bazant size-effect model and to the Jenq-Shah two-parameter model.

Each main section is divided into three subsections: (1) The theoretical background of each approach is briefly explained; (2) the experimental aspects related to the measurement of the relevant parameters of this approach are discussed; and (3) the most relevant output of these models—the prediction of the size effect in maximum load—is considered.

It is found that the cohesive crack model is able to explain and to predict most of the experimental results with concrete samples. Also, it happens that inside a range of usual sizes, cohesive crack models can be approximated by equivalent elastic crack models with their associated R-Δa curve. Bazant's and Jenq-Shah's two-parameter models can be considered as limiting examples of this approach. For very large sizes, one can approximate all these models by the simple LEFM model. Using this scheme, one can see that most of the known models appear related in a hierarchical way.

Many details were omitted to keep this overview to a reasonable length. Proofs and computations appear in the references that reflect work done by the authors during the last 5 years.

The Cohesive Crack Model Approach

Theoretical Background

The first cohesive crack models appeared as an alternative to LEFM to eliminate the stress singularity [17,18]. Hillerborg generalized the concept of process zone, removing the small nonlinear zone requirement [1], and, more recently, the authors have shown that this model may be considered as a particular case of continuum mechanics nonlocal formulation [19]. A review of the

Address correspondence to: Manual Elices, Departmento de Ciencia de Materiales, Universidad Politécnica de Madrid, ETSI Caminos, Ciudad Universitaria, 28040 Madrid, Spain.
Received January 8, 1996; Accepted July 24, 1996

ISSN 1065-7355/96/$15.00
PII S1065-7355(96)00072-7

relevant properties of this model was done by the authors in some recent papers [20,21] and by Carpinteri [3]. The basic concepts are summarized in the following discussion.

A cohesive crack model is characterized by the properties of the bulk material, the crack initiation condition, and the crack evolution function. The simplest assumptions are:

1. The bulk material behavior follows a linear elastic and isotropic stress-strain relationship, with elastic modulus E and Poisson's ratio ν. This assumption is not essential but makes computations easy. The bulk material can be modeled as nonlinear elastic or elastoplastic depending on the problem considered.
2. The crack initiates at a point where the maximum principal stress σ_I at that point reaches the tensile strength f_t. Moreover, the crack forms normal to the direction of the major principal stress.
3. After its formation, the crack opens while transferring stress from one face to another. The stress transferred—the *cohesive stress*—is a function of the crack opening displacement history. For monotonic mode I opening, the stress transferred is normal to the crack faces and is a unique function of the crack opening:

$$\sigma = f(w) \tag{1}$$

The function $f(w)$ is called the *softening function* or softening curve. This is the simplest form of this function and may depend on triaxiality and other parameters.

For concrete and cementitious materials, the softening function is a nonincreasing function of the crack opening, as depicted in Figure 1. The main features of this curve are the following:

1. The tensile strength f_t is the stress transferred at the incipient opening.
2. The initial slope is measured as f_t/w_1. For not-too-large cracked specimens and for uncracked specimens of any size, these two parameters suffice to predict maximum loads [22,23]. This is so because at maximum load, the crack is not yet fully open—this happens only for cracked specimens of infinite size—and only the initial part of the softening curve is active (see the section on Determination of the Initial Linear Softening).
3. The specific fracture energy G_F is the work needed to bring completely apart the two faces of a unit surface of crack and is represented by the area under the softening curve. If the softening function is a material property, this area is a constant and a material property as well. Deviations of G_F from a constant value reflect more involved softening functions, depending on additional variables apart from w.
4. The critical crack opening w_c is the crack opening for which the stress transferred becomes zero.

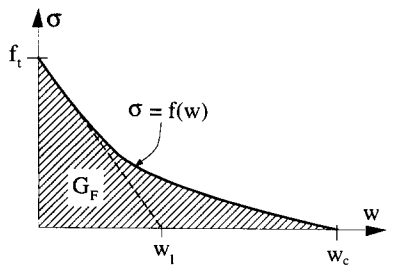

FIGURE 1. Softening curve and initial linear approximation.

Experimental Aspects

DETERMINATION OF THE SOFTENING FUNCTION. The softening function is the key ingredient for cohesive crack models. Direct tensile tests should provide, ideally, the whole softening curve jointly with the tensile strength of the concrete. Experimental measurement of this curve may be done from a stable tensile test, if a *single* crack is formed and opened keeping its faces parallel, as done by Petersson [24]. However, this test is very difficult to perform and its interpretation is not straightforward, mainly because the test tends to shift to asymmetric modes of failure or because several cracks develop simultaneously.

The softening function can be obtained also from the underlying theory of cohesive cracks, using an indirect J-integral technique, as proposed by Li et al. [10]. Although theoretically elegant, this method is hardly applicable to concrete, because it involves subtraction of load-displacement curves for specimens with only slightly different notches, a procedure that multiplies the experimental errors so that the final result loses significance.

Inverse procedures that ascertain the softening curve from load-displacement or load-crack mouth opening displacement (CMOD) curves of notched specimens are increasingly used. Wittmann and Mihashi use such a procedure by postulating a four-parameter bilinear softening curve and determining these parameters by best-fitting to measured load-deflection curves of stable tests on notched specimens [12,25,26]. A similar procedure has also been used by Ulfkjaer and Brincker [27]. Another procedure, based again on cohesive crack models, was recently proposed by Uchida et al. [28]. A polylinear softening function was obtained from the load-displacement values of a three-point bending test of a notched beam in conjunction with an optimization algorithm.

Advn Cem Bas Mat
1996;4:116–127

Quite often, a simplified procedure assuming that the softening curve can be approximated by a bilinear function suffices, as sketched in Figure 2. The four needed parameters can be obtained from the results of two tests, cylinder splitting and three-point bending of notched beams [29].

Although the full softening curve is required to completely define a cohesive crack model, in some special situations, partial information about it is enough to make predictions of engineering value. This is the case for peak-load determination for very large sizes and for relatively small sizes. In those situations, simplified experiments can suffice to get valuable information.

DETERMINATION OF FRACTURE ENERGY. When the size of the structure is much larger than the cohesive zone size, LEFM is a reasonable first-order approach to the cohesive crack model. In this limit (in which both the crack length and the uncracked ligament must be very large), the peak load is fully controlled by the fracture energy G_F, and thus an experimental setup to determine only this parameter is of practical interest.

The fracture energy can be measured using the procedure described in the RILEM draft recommendation [30] that consists of measuring the external work supply required to break the specimen in a stable test on a notched beam. The work supply divided by the initial ligament equals G_F.

However, it appears that direct application of this procedure delivers measured values of G_F that are size dependent. The authors have been working on this problem and have shown that a number of spurious energy dissipation sources may be present during one of those tests: hysteresis of the testing arrangement, dissipation in the bulk of the specimen, dissipation by crushing at the supports, and neglect of the final portion of the load-displacement curve. When all these factors are properly taken into account, the size effect of the experimental values is strongly decreased [31–33].

The observed size dependence of G_F for some concretes still deserves further research, with, possibly, three ways of analysis: (1) to extend the cohesive crack model to include parameters not yet considered, such as multiaxiality; (2) to include the possibility of a size effect introduced by the random nature of the material (statistical size effect); and (3) to seek evidence of the intrinsic unsuitability of the cohesive crack model for concrete and to provide a completely new approach. At this moment, it seems that the experimental evidence is not enough to make a reasonable choice of alternatives; more extensive and accurate experimentation is needed.

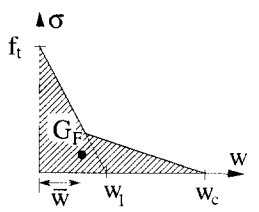

FIGURE 2. Bilinear approximation of the softening curve. The heavy dot represents the center of gravity of the dashed area.

If the full σ-w curve is determined following any of the procedures mentioned in the previous section, G_F can be determined as the area enclosed under the σ-w diagram. However, if only G_F is sought, then the RILEM work-of-fracture method is much easier to carry out.

DETERMINATION OF THE INITIAL LINEAR SOFTENING. In many practical cases, the peak load is completely determined by the tensile strength and the slope of the initial portion of the softening curve. This is so for notched specimens of laboratory sizes [22] and for unnotched specimens of all sizes [23,34]. Figure 3 sketches the reason for this property: For relatively small specimens, when the peak load is reached, the stress profile along the ligament is as shown in Figure 3a, which means that no point on the specimen has softened further than the circled point in Figure 3b. Therefore, at peak point, the results for the actual softening curve (full line) and for the linear approximation (dashed line) are indistinguishable.

This property can be used to determine the initial straight part of the softening curve (which depends only on two parameters) from the measurement of the peak load of two specimen types. Up to now, the authors have used the cylinder splitting strength (which is taken to give a good estimate of the tensile strength) and the peak load for a notched three-point bend beam from which the horizontal intercept w_1 is determined [29].

Size-Effect Predictions

GENERAL SIZE-EFFECT PROPERTIES. The change of a structural property when the size of a structure increases is known as a *size effect* related to this property. The most important size effect for the designer is the one related to the maximum load a structural element can withstand, and the cohesive crack model allows the prediction of such size effect for notched and unnotched structural elements.

Figure 4 shows computed results for the maximum load (expressed in terms of K_{INmax}) as a function of intrinsic size (D_i) for a concrete with a bilinear softening function. This plot deserves some attention because the coordinates are not conventional: The maximum load appears as $E'G_F/K^2_{INmax}$; where E' is the generalized Young's modulus and G_F is the specific fracture energy

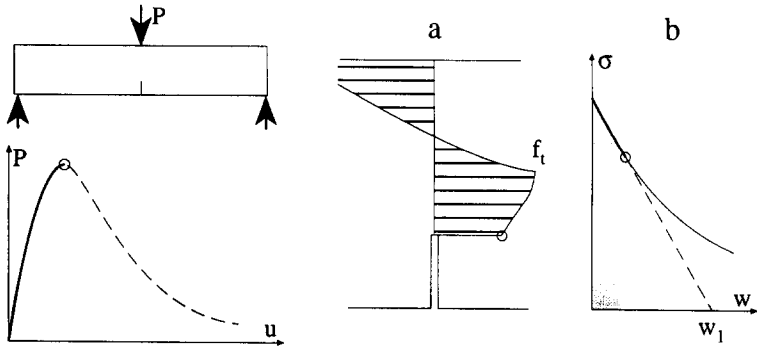

FIGURE 3. Notched beam in three-point bending at peak load. (a) Stress profile along the ligament. (b) Situation on the softening curve of the material at the notch tip.

(already defined as the area under the softening curve), and

$$K_{IN} = S(a_0/D)\,\sigma_N\sqrt{D} \tag{2}$$

where σ_N is a nominal stress, $\sigma_N = 3\,PS/2BD^2$ (P, S, B, D and a_0 are shown in the insert of Figure 4), and $S(a_0/D)$ is a shape factor [8]. The size appears as l_{ch}/D_i, where

$$l_{ch} = E'G_F/f_t^2 \tag{3}$$

is Hillerborg's characteristic length and the intrinsic size D_i is defined as

$$D_i = \frac{S(a_0/D)}{2S'(a_0/D)}D = \left(\frac{\partial \ln K_I^2}{\partial a}\right)^{-1}_{a=a_0} \tag{4}$$

One advantage of the intrinsic size is that it is independent on the choice of the dimension D, as is shown from the second equality in eq 4. The use of stress intensity factors in eqs 2 and 4 does not imply, by any means, using LEFM, it is only a convenient way to relate P and D.

The plot of Figure 4 is quite general (i.e., it is almost the same) for usual positive geometries and normal concrete as was shown by the authors [29,35,36].

SIZE EFFECT IN THE LARGE SIZE RANGE. Consider a concrete specimen with a characteristic dimension (a size, for short) D and assume that the fracturing behavior is well described by a cohesive crack model. Under this hypothesis, a cohesive crack grows ahead of the initial crack tip. The size of the cohesive zone is denoted by c. When the whole cohesive zone can be lumped in a single point ahead of the crack tip (a necessary condition is $c/D \ll 1$), LEFM can be applied. Under these circumstances, all the details of the softening function disappear and only G_F, the area under the softening curve, remains as the relevant parameter.

As is well known from LEFM, if this approximation is valid, there is an autonomous region around the crack tip where the stress and strain fields depend on only one parameter: the stress intensity factor K. In other words, once K is known, the stress and strain fields are known. Moreover, there is a critical value of K, the fracture toughness K_C, that when reached the crack starts propagating. Fracture toughness is related to specific fracture energy through the well-known relation $K^2 = E'G_F$.

This approach was analyzed in detail by the authors in two papers [37,38]. One important result was that for a cracked sample (initial crack length a_0) of a cohesive material loaded under mode I, *every far field may be approximated, up to order c/D, by the far field corresponding to an equivalent elastic crack of length* $a_0 + \Delta a_\infty$ (as shown in Figure 5).

In the statement of this theorem, subscript ∞ for Δa indicates that large-size asymptotics is considered. A procedure for computing Δa_∞ was given in Planas and Elices [37] and a lower bound for Δa_∞ was also derived. In particular, it was found that when the crack tip opening displacement reaches the critical crack opening value w_c, the critical cohesive zone size c_c and the effective crack extension Δa_∞ verify

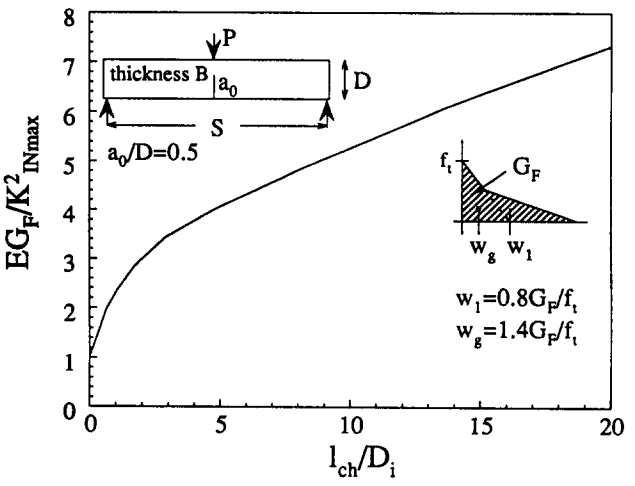

FIGURE 4. Size-effect curve for a three-point bent notched beam and a material displaying bilinear softening.

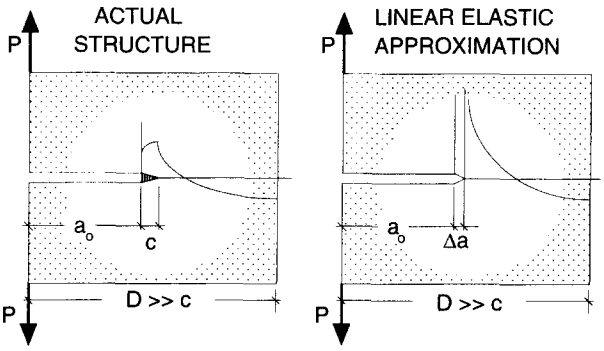

FIGURE 5. Effective crack extension in the infinite size limit. The remote fields (shaded areas) are the same to order c/D.

$$c_c \geq \Delta a_{\infty c} \geq \frac{\pi}{32} w_c^2 \frac{E'}{G_F}. \tag{5}$$

It was shown, moreover, that for the usual softening shapes, the actual value of $\Delta a_{\infty c}$ is very close to the lower bound, that is,

$$\Delta a_{\infty c} \approx \frac{\pi}{32} w_c^2 \frac{E'}{G_F}. \tag{6}$$

As mentioned in the previous section, the maximum load size effect for cohesive materials can be conveniently analyzed using the variables $E'G_F/K^2_{INmax}$ and l_{ch}/D_i. The general trend was sketched in Figure 4. This representation has the advantage of bringing the infinite size into focus near the origin.

Based on the asymptotic analysis, the authors have shown that for large sizes—when $(l_{ch}/D_i)^2$ is negligible in front of l_{ch}/D_i—the size effect for maximum load takes the simple form [37]

$$\frac{E'G_F}{K^2_{INmax}} = 1 + \frac{\Delta a_{\infty c}}{D_i}. \tag{7}$$

As an example, the size dependence of the maximum load was analyzed for notched beams made with three different cohesive materials and numerically tested in three-point bending. The beams had a span-to-depth ratio of 4 and an initial notch-to-depth ratio of 0.5. The results are sketched in Figure 6, together with the first-order approximation (7), for three different softening functions. The corresponding effective crack extensions were $\Delta a_{\infty c} = \pi l_{ch}/24$ for rectangular softening, $\Delta a_{\infty c} \approx 0.419\ l_{ch}$ for linear softening, and $\Delta a_{\infty c} \approx 2.48\ l_{ch}$ for quasi-exponential softening. (for more details, see ref 8).

The Equivalent Elastic Crack Approach

The size of most usual structural concrete elements is not large enough to admit the simplified LEFM approach, and, in general, one has to resort to involved numerical techniques for solving the nonlinear problems posed by the cohesive crack model. The equivalent elastic crack approach (EEC) emerges as an intermediate technique to avoid cumbersome computing while still using the simple LEFM procedures with an associate R curve. This approach is not always legitimate, and its justification and limitations are briefly summarized in the following discussion.

Theoretical Background

GENERAL THEORY OF EQUIVALENT CRACKS. The equivalent elastic crack greatly simplifies the computations by

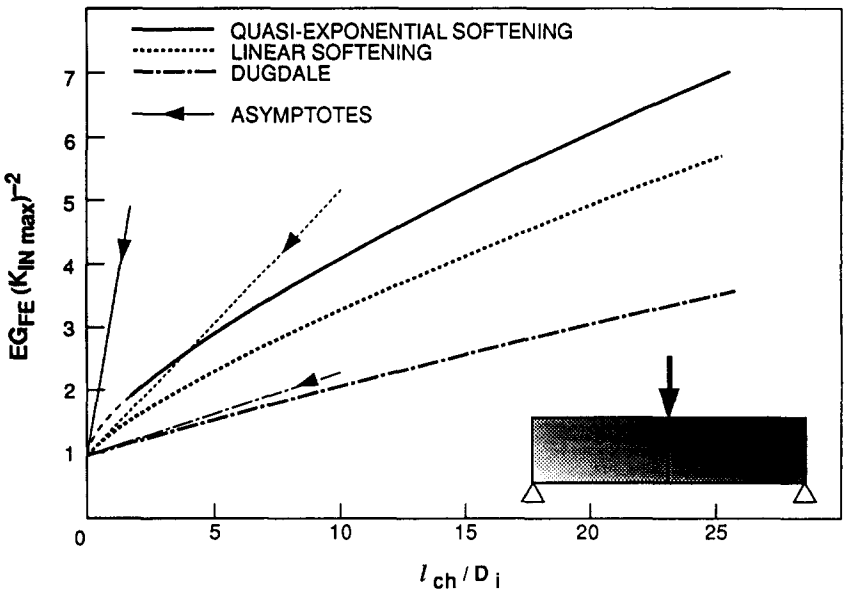

FIGURE 6. Size-effect plot for the maximum load, showing first-order asymptotes, for three shapes of the softening curve. "Dugdale" refers to rectangular softening, equivalent to a Dugdale model with cutoff.

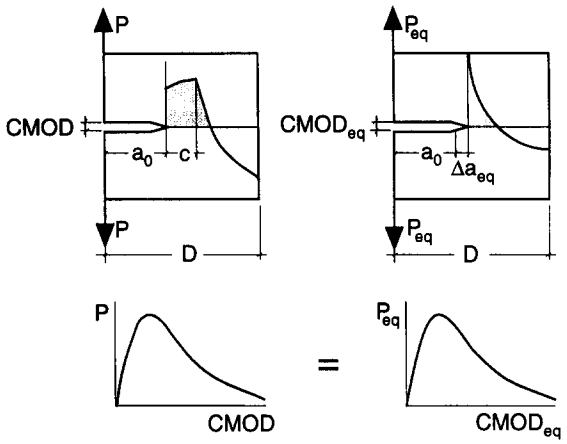

FIGURE 7. Actual, cohesive material specimen (left) and equivalent linear elastic specimen (right). Equivalence is set by forcing identical *P-CMOD* response. CMOD = crack mouth opening displacement.

shifting from a cohesive material (and, hence, a nonlinear structural analysis) to a linear elastic material (which only requires linear analysis). The unified concept of equivalent elastic crack, as described in this section, was developed by the authors in two papers [39,40]. First, the more familiar equivalences based on load, the so called *P-Y* equivalences, are reviewed and then the general *X-Y* equivalences are considered.

The concept of elastic equivalence is best illustrated on a particular example. Let us choose the force-crack mouth opening displacement equivalence or *P-CMOD* equivalence. As shown in Figure 7, two geometrically identical cracked samples are loaded under CMOD control. One sample is made from a cohesive material and the other (the equivalent) from a linear elastic material. The measured loads in the two samples, P and P_{eq}, for the same *CMOD* will be different, but we can force the loads to match each other ($P = P_{eq}$), at each value of *CMOD*, by choosing a suitable equivalent crack length a_{eq} and a suitable crack growth resistance R_{eq}.

In this way, we force both samples to exhibit the same *P-CMOD* behavior, but generally the equivalence ends here; the stress field, for example, need not be the same, as seen in Figure 7. The price paid for the forced equivalence is that the linear elastic material does not have a *constant* toughness (G_F is constant for the cohesive material and for the LEFM approach) but rather has a changing resistance—an R-Δa curve. This curve, in general, is not a material property but depends on the geometry and specimen size.

As an example of the application of the load-*CMOD* equivalence, imagine we want to predict the load-*CMOD* of a cracked panel in tension made from a cohesive material, using the test results of a three-point notched beam made of the same material. The procedure to compute the load-*CMOD* for the cracked panel is as follows: The *P-CMOD* is first measured from the beam test, from which the corresponding R-Δa curve is derived. Then, assuming that the R curve is a material property, a *P-CMOD* curve for the notched panel is predicted under the simplified assumption of linear elastic behavior. The prediction is shown in Figure 8a for a panel of the same depth as the beam used to determine the R curve. The agreement of the prediction and the experimental result is excellent. In this example, the experimental results are numerically computed using the cohesive crack model, because the experimental values are assumed to be indistinguishable from numerical computations based on cohesive cracks. However, if the relative sizes and notch depths of both structures are quite different, the agreement can be rather poor, as shown in Figure 8b. More details about this example and the validity of the assumptions implicit in the R curve approach can be found in ref. 39 and 40.

Apart from the *P-CMOD* equivalence, other *P-Y* equivalences may be sought (where *Y* stands for other possible magnitudes). For example *P-u*, *P-CTOD*, or *P-J* equivalences, where *u*, *CTOD*, or *J* are, respectively, the displacement associated with *P*, the crack tip opening displacement, or the *J* integral.

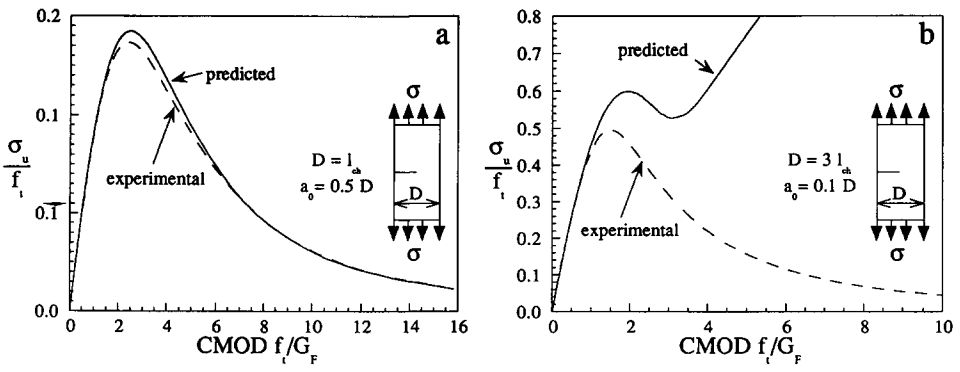

FIGURE 8. Comparison of the experimental response (cohesive behavior) of a single edge notch panel in tension (SENT) to its response predicted using the R-Δa curve determined from a *P-CMOD* equivalence for a three-point bend beam (TPB) with a depth $D = l_{ch}$ and a notch-depth ratio of 0.5. (a) SENT specimen with dimensions similar to those of the TPB specimen. (b) SENT specimen with dimensions differing largely from those of the TPB specimen. CMOD = crack mouth opening displacement.

Advn Cem Bas Mat
1996;4:116–127

The concept of *P-Y* equivalence can be generalized to any controlling variable, not necessarily the load *P*, and the same procedure can be extended to any pair of variables *X-Y*. This generalization permits one to consider apparently unrelated procedures within the same framework, such as Bazant's *R-Δa* approach [41] or the *J-CTOD* approach [38]. Further details may be gleaned from Elices and Planas [39] and Planas et al. [40].

BAZANT'S SIZE-EFFECT-BASED MODEL. Bazant introduced a procedure for computing a size-independent (although, geometry-dependent) *R-Δa* curve from the knowledge of the maximum load size-effect curve. The equivalence is imposed by stating that for geometrically similar bodies the peak load must be the same in the actual and equivalent specimen for every size *D*, that is, $P_{max} = P_{eq.max}$. This is equivalent to saying that the size-effect curves for the actual and the equivalent specimen are made to coincide, in much the same way as the *P-CMOD* curves are made to coincide in the *P-CMOD* equivalence; in this sense, Bazant method can be called a P_{max}-*D* equivalence.

The general procedure put forward by Bazant et al. [41] to obtain the *R-Δa* is summarized by the following property: Given the size-effect curve as

$$P_{max} = P_{max}(D) \tag{8}$$

the *R-Δa* curve is the envelope of a uniparametric family of curves, with parameter *D*, given by

$$R^{BG} = \frac{1}{E'}\left[\frac{P_{max}(D)}{B\sqrt{D}}\, S\left(\frac{a_0 + \Delta a^{BG}}{D}\right)\right]^2 \tag{9}$$

where superscript *BG* stands for Bazant and General, because no particular size-effect curve is postulated here.

The size-effect equation (eq 8) may come from a cohesive model, from Bazant's size-effect law, or from any other model. The result depends on $P_{max}(D)$ and also on a_0/D and other hidden geometrical parameters, implicit in the shape function *S*. The resulting *R* curve is size independent, because *D* is eliminated in finding the envelope of eq 9; but it is geometry dependent because the shape function *S* is geometry dependent.

In Bazant's model, the size-effect relation eq 8 is taken to be the Bazant law, which can be written as

$$\frac{E'G_{FB}}{K^2_{INmax}} = 1 + \frac{c_f}{D_i} \tag{10}$$

where D_i is the intrinsic size defined in eq 4. (Note the similitude of eqs 10 and 7. Both are straight lines in the plot of Figure 4). This size effect depends only on two fracture parameters, namely

$$G_{FB} \text{ and } c_f \tag{11}$$

where G_{FB} stands for the fracture energy computed for Bazant's model (which differs from G_F, the area under the softening function of the cohesive model) and c_f is the critical crack extension for infinite size.

Given these two parameters, Bazant and Kazemi [42] showed that the *R* curve can be determined in closed parametric form for any given geometrical shape. The shape of the *R*-curve is as shown in Figure 9. Note that (c_f, G_{FB}) are the coordinates of the point *M* at which the tangent to the *R* curve becomes horizontal.

JENQ-SHAH TWO-PARAMETER MODEL. The model of Jenq and Shah [43] is also an equivalent elastic crack model, but it is only partial because, if no further hypotheses are set, the model refers only to the peak load and no *R* curve can be inferred from it. The two parameters of Jenq-Shah model are

$$K^S_{IC} = (E'G_{FS})^{1/2} \text{ and } CTOD_{CS} \tag{12}$$

It is assumed that a slow crack growth takes place under increasing load up to a certain crack extension Δa_c at which the maximum load is attained. This critical situation is assumed to occur when, simultaneously, the stress intensity factor at the equivalent crack tip reaches its critical value K^S_{IC} and the crack tip opening at the initial crack tip reaches its critical value $CTOD_{CS}$ where index *S* refers to the Jenq-Shah model.

Strictly speaking, the Jenq-Shah model as originally formulated only states the conditions for peak load. No explicit statement is made regarding the crack evolution before and after the peak; this means that no *R-Δa* curve is postulated. In principle, infinite geometry-dependent *R-Δa* curves exist that satisfy Jenq-Shah model (i.e., that give the same peak load and *CTOD* as the Jenq-Shah model). One particular *R* curve emerges, if the envelope method explained in the previous section is used, as done by Ouyang et al. [44] and Ouyang and Shah [45]. These authors computed the *R* curve as the envelope of the family of curves given by eq 9 with

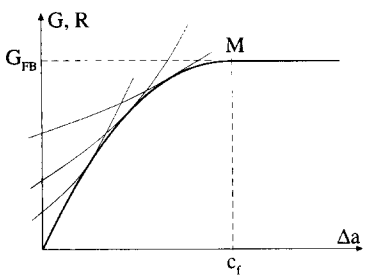

FIGURE 9. Sketch of the *R-Δa* curve for Bazant's model. The thin line curves represent *G-Δa* curves at peak load for different sizes.

$P_{max}(D)$ equal to the peak load predicted by the Jenq-Shah model. However, different from Bazant's approach in which geometrically similar specimens are considered so that a_0/D = const., in the analysis of Ouyang et al., a constant initial crack size is considered (a_0 = const). This method delivers a geometry-dependent R-Δa curve that can be computed once the two parameters K_{IC}^S and $CTOD_{CS}$ have been determined. We will see later that in experiments, a *P-CMOD* equivalence is used to determine these parameters.

The Jenq-Shah conditions for peak load can be also interpreted in terms of the singular *R-CTOD* curve shown in Figure 10 in which the point *M*, of coordinates ($CTOD_{CS}$, G_{FS}), is a cusp. The dashed part of the curve is not known in detail, but it is not required to determine the peak load, because, for well-behaved geometries, the peak-load condition always occurs at the cusp point. This is the Jenq-Shah condition. This is so because the peak load occurs when the *G-CTOD* curves at constant load become tangent to the *R-CTOD* curve; and because there is a cusp point at *M*, this is the critical point, as illustrated in Figure 10, in which the set of thin lines represent the *G-CTOD* curves at constant load.

Just a few words to remark that the *R-CTOD* formulation can be used in general as an alternative of the R-Δa formulation. In fact, for a given geometry and size, there is a one-to-one correspondence between the two, dictated by the LEFM relations. If the *R-CTOD* curve is size and geometry independent, the R-Δa curve is not, and reciprocally. Planas et al. [46] showed that the size effect in concrete specimens can be captured quite acceptably by size-independent *R-CTOD* curves (see also ref. 40 for a justification of the use of the *R-CTOD* curves based on cohesive cracks and a *J-CTOD* equivalence, in which *J* is Rice's *J*-integral).

Experimental Aspects

GENERAL METHOD FOR DETERMINATION OF THE *R* **CURVE.** The use of crack growth resistance curves, R-Δa, to predict

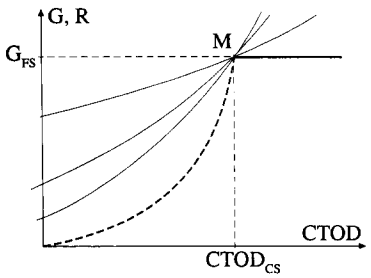

FIGURE 10. Sketch of the *R-CTOD* for Jenq-Shah model. The dashed portion of the curve is not required to determine the peak load. The thin line curves represent G-Δa curves at peak load for different sizes and geometries. CTOD = crack tip opening displacement.

the behavior of cracked specimens is a well-established practice for ceramics, cementitious, and other quasi-brittle materials. *R* curves may stem from two quite different sources, and it is worthwhile to keep this in mind when dealing with them. One source is due to the evolution of the physical mechanisms operating during crack growth, such as plasticity in metals or transitions from one fracture mode to another with crack growth. The second source is a fictitious fracture resistance increase due to the *elastic crack equivalence*, as explained before. In what follows, only the second source will be considered to be consistent with the cohesive crack model, where G_F is constant and a material property.

For computing the R-Δa curve, one can proceed as follows: First, the equivalent elastic crack length is deduced (consider, again, the example based on the *P-CMOD* equivalence; for other equivalences, the procedure is similar). From the measured *P* and *CMOD* values, the equivalent elastic crack length a_{eq} is derived from the expression of the compliance for the equivalent elastic sample

$$C_{eq}(a_{eq}) = CMOD/P \tag{13}$$

Then the corresponding stress intensity factor is computed from LEFM

$$K_{Ieq} = \frac{P_{eq}}{B\sqrt{D}} S\left(\frac{a_{eq}}{D}\right) \tag{14}$$

where *B* is the specimen thickness, *D* is one of its characteristics in-plane dimensions, and $S(a/D)$ is the geometrical shape factor.

Finally, the R-Δa curve is established from the well-known relation

$$R(\Delta a_{eq}) = \frac{1}{E'}\left[K_{Ieq}(P_{eq}, a_0 + \Delta a_{eq})\right]^2 \tag{15}$$

where the equivalent crack length was written explicitly as $a_{eq} = a_0 + \Delta a_{eq}$ to emphasize its dependence on the crack increment.

Notice that this R-Δa curve is dependent not only on the chosen equivalence but also on the size and geometry of the specimen, because of the implicit size and geometry dependence of Δa_{eq}. Figure 11 shows different R-Δa curves corresponding to several equivalences, all for the same geometry. The predictive capabilities of equivalent elastic crack models depend on how good the assumption is of a constant (material property) R-Δa curve. For some geometries and sizes, this assumption is good, but this can never be taken for granted [39,40].

The possibility also exists of obtaining R-Δa curves as envelopes of G-Δa curves at peak load for varying size (see sections on Bazant's Size-Effect-Based Model and

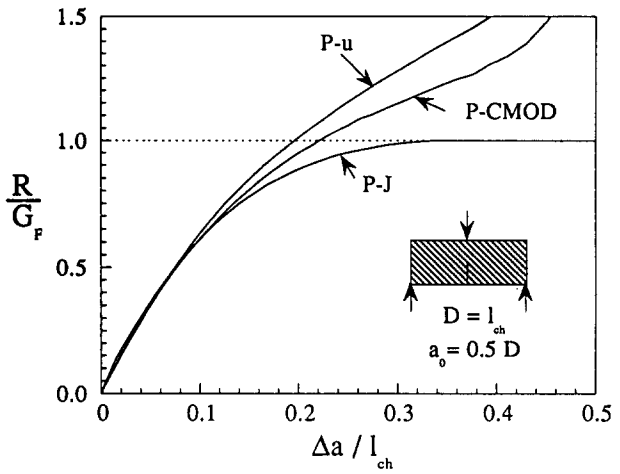

FIGURE 11. *R-Δa* curves for three different equivalences: *P-u*, *P-CMOD*, and *P-J*. CMOD = crack mouth opening displacement.

Jenq-Shah Two-Parameter Model for the general aspects of the method; detailed procedures can be found in the original papers, refs 42 and 44.)

DETERMINATION OF BAZANT'S FRACTURE PARAMETERS. In Bazant's approach, the size effect is first determined and then the *R-Δa* can be computed for any geometry following the analytical procedure devised by Bazant and Kazemi [42].

The usual experimental determination consists in testing notched beams of various sizes for peak load and then making a two-parameter curve fit of Bazant's size-effect law to the experimental results. The detailed procedure is described in a draft recommendation from RILEM [47].

DETERMINATION OF JENQ-SHAH FRACTURE PARAMETERS. The two parameters of the Jenq-Shah model can be determined by measuring the load and *CMOD* at the peak for a notched geometry and size. From these two values, the effective crack extension at peak is determined from LEFM relations. Then the value of K_I and *CTOD* at peak are determined also from LEFM relations. These values must coincide, by definition, with the two parameters K_{IC}^S and $CTOD_{CS}$.

In practice, the procedure is more involved, because the inelastic part of the CMOD is removed by making an unloading-reloading loop just after the peak and using the unloading-reloading compliance to determine the elastic part of the CMOD. This is inserted in the LEFM formulae, and the computation follows as previously indicated. Detailed procedures are described in a draft recommendation by RILEM [48].

Size Effect Predictions

GENERAL EQUIVALENCES. If one makes the assumption that the *R-Δa* curve is universal, that is, geometry and size independent, it can be used to predict the size effect for any geometry. The procedure to follow to extract the size-effect curve from the postulated *R-Δa* curve was shown in detail in Elices and Planas [49].

Likewise, if the *R-CTOD* curve is assumed to be universal, then the size-effect curve can be determined for any geometry. This procedure, with the *R-CTOD* curve based on a *J-CTOD* equivalence was analyzed by Planas et al. [46] with good results. The only drawback of this analysis is that the computational procedure is much more involved, because closed form expressions for the (elastic) CTOD are not common.

Interestingly enough, all the equivalent models, either based on *R-Δa* or *R-CTOD* curves, lead to equations that for large size converge to the asymptotic eq 7 for the cohesive crack and to Bazant's size-effect law (eq 10), except, of course, that the values of the parameters are different for the various models.

SIZE EFFECT IN BAZANT'S MODEL. Once the parameters G_{FB} and c_f have been determined, the size-effect curve in Bazant's approach is given by eq 10 for any geometry. There is a dependence of geometry embodied in the geometrical shape factor S appearing in the definitions of K_{IN} and D_i.

It is interesting to see how the size-effect predictions of the cohesive model and of the Bazant model compare to each other. This analysis was developed by the authors, with the results shown in Figure 12 [50]. The fitting of both models over the practical size range is very good, giving maximum differences between the two models of less than 2.5%, which makes it practically impossible to distinguish experimentally which of the two models is more appropriate. To detect appreciable differences (of about 10% of maximum load), one needs to increase the experimental size range to beams of more than 1-m depth. However, the extrapolations to very large sizes do diverge appreciably, Bazant's model being more conservative by about 30%.

SIZE EFFECT IN JENQ-SHAH MODEL. Determining the size effect predicted by the Jenq-Shah model is more involved. It can be written in parametric form [50] as

$$\frac{E'G_F}{K_{INmax}^2} = \frac{G_F}{G_{FS}}\left[\frac{S[(a_0+\Delta a_c)/D]}{S(a_0/D)}\right] \tag{16}$$

$$\frac{l_{ch}}{D} = \frac{l_{ch}}{\Delta a_{\infty CS}}\frac{\Delta a_c}{D}\left[L\left(\frac{a_0+\Delta a_c}{D}, \frac{\Delta a_c}{D}\right)\right]^2 \tag{17}$$

where the parameter is $\Delta a_c/D$, G_{FS} is as defined in eq 12, $S(a/D)$ is the shape factor already mentioned, $L(a/D, \Delta a_c/D)$ is a regular function related with the crack opening displacement that may be determined from elastic analysis as shown in Planas and Elices [50], and

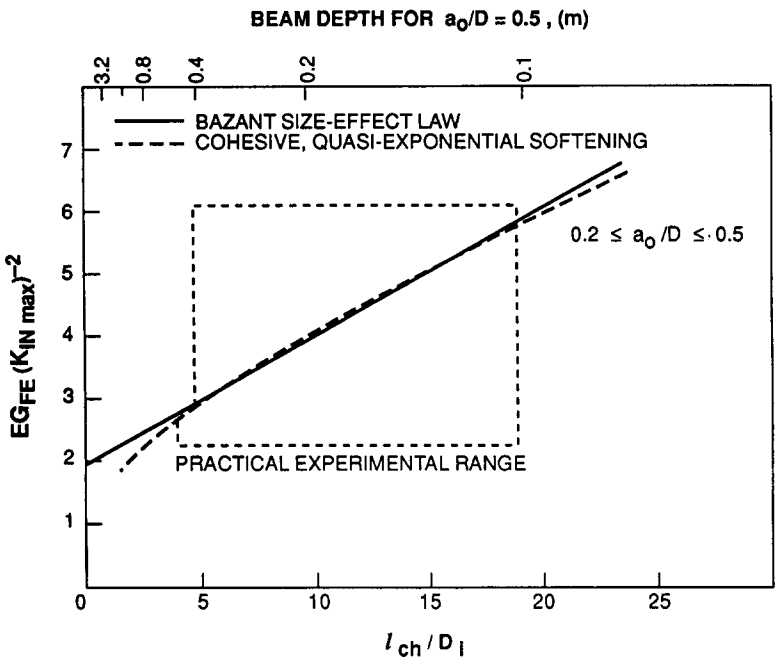

FIGURE 12. Comparison of Bazant's size-effect curve and the size effect predicted for a cohesive model.

$\Delta a_{\infty C,S}$ is the critical effective crack extension for infinite size in the Jenq-Shah model, which is related to the basic Jenq-Shah parameters by

$$\Delta a_{\infty C,S} = \frac{\pi}{32}\left(\frac{CTOD_{cs}E'}{K_{IC}^{S}}\right)^2 \tag{18}$$

To compare the size effect predicted by this model to that predicted by the cohesive crack model, we performed an analysis similar to that presented before for Bazant's model. The results are shown in Figure 13 [50].

The differences in maximum load as predicted by the two models is again very low on the practical experimental size range. The models diverge again for large sizes, where Shah's model is more conservative by about 30%.

Correlation Between the Parameters of the Various Models

The results of Figure 12 and 13 provide a sound basis for establishing a correlation between the parameters of

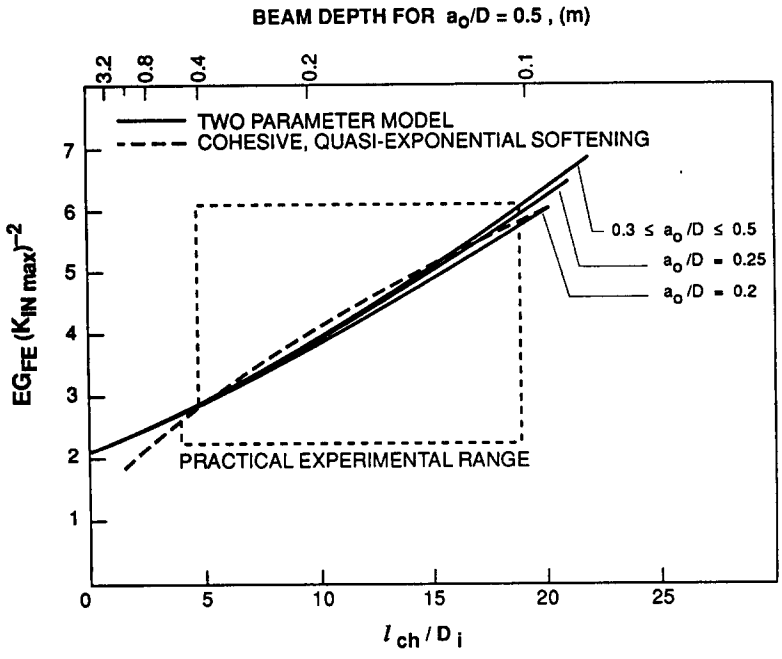

FIGURE 13. Comparison of the size effect predicted by the Jenq-Shah model and the size effect predicted for a cohesive model.

Advn Cem Bas Mat
1996;4:116–127

the various models. The method requires one to see which set of parameters give approximately the same peak load for notched specimens of typical laboratory size. The correlation is of course not exact, because the range of sizes so defined is relatively vague. However, for ordinary concrete, the variability is narrow enough for these correlations to be useful as first approximations.

In Planas and Elices [50], the correlation between the various parameters was established using G_F and l_{ch} as the basic parameters for the cohesive model. It turned out, then, that the correlation was dependent on the shape of the softening curve. Subsequently, we realized that for the usual experimental range of sizes the peak load for the cohesive model is completely defined by the initial linear softening.

Therefore, if one searches to correlate the results with the tensile strength f_t and the horizontal intercept w_1 (Figure 1), the resulting correlation has to be nearly universal. It turns out that the results in Planas and Elices [50] can be readily transformed by using the result (derived in ref 37) that for quasiexponential softening the fracture energy is related to f_t and w_1 by

$$G_F = 0.86\, f_t\, w_1 \tag{19}$$

from which the characteristic length follows as

$$l_{ch} = 0.86 \frac{E' w_1}{f_t}. \tag{20}$$

Inserting the preceding relations in the results in Planas and Elices [50] the following correlations stem out:

$$G_{FB} \approx 0.45\, f_t w_1,$$

$$c_f \approx 0.094 \frac{E' w_1}{f_t} \quad \text{for Bazant model} \tag{21}$$

$$G_{FS} \approx 0.41\, f_t w_1,$$

$$CTOD_{CS} \approx 0.52\, w_1 \text{ for Jenq–Shah model.} \tag{22}$$

These correlations hold within a few percent for size ranges of the order of 12 to 40 cm for ordinary concrete and notched specimens. If they have to be used for other materials (high strength concrete or mortar), the appropriate range is expressed in terms of the intrinsic size as

$$D_i \approx 0.05 \text{ to } 0.2 \frac{E' w_1}{f_t} \tag{23}$$

Final Comments

The cohesive crack model was proven useful in explaining most experimental results and general enough to encompass other crack models. It was shown that more simple models can find their place inside the frame of the cohesive model, allowing a unified language and relations between them to be established. More involved models can also be related to the cohesive one. For those who believe that only nonlocal models are worth being considered, it was shown that the cohesive model can be considered as a special case of a family of integral nonlocal models [19]. The hierarchy among these models is summarized in Figure 14.

It seems that for usual laboratory sizes and geometries most of the approaches bring similar results regarding the maximum load, particularly those based on two parameters. The correlations shown in eqs 21 and 22 provide a means of comparing and unifying experimental results obtained by different experimental methods. Note that previous correlations depended on the shape of the softening curve. Today, we know that because only two parameters of the softening curve—tensile strength f_t and initial slope (or equivalently w_1)—control the peak load for typical laboratory specimens, the foregoing correlations are "nearly" unique.

For very large sizes and notched or cracked specimens, LEFM is a valid approximation. When maximum load is reached, almost the whole softening curve has been used. In these circumstances, the relevant parameter is G_F, the area under the whole curve. Note that the previous results indicate that the parameters of the Bazant model and the Jenq-Shah model *do not* correlate with G_F. This is so because they use only peak-load values. For normal specimen loads, the peak is reached without much softening, so that no information about the tail of the softening curve can be obtained (see Figure 3). However, accumulated experience indicates that the total area under the softening curve for ordinary concrete is close to $f_t w_1$. This is only a rule of thumb,

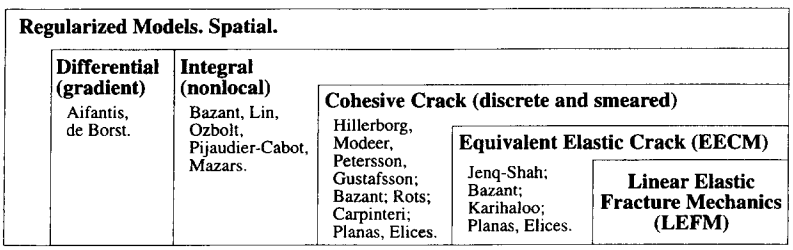

FIGURE 14. Hierarchical organization of the various models used to describe the fracture of concrete.

and 25% deviation can easily be found for particular concretes.

Models will settle with time, and those with more predictive capacity for different geometries and sizes and those that are easier to use will survive. It is hoped that this reference frame will be useful in keeping track of the evolution of the various models.

Acknowledgments

This paper is an expanded version of an invited talk at the workshop on *Fracture Mechanics Parameters of Concrete* organized by Profs. Ben I.G. Barr and S.E. Swartz in Cardiff U.K., July 1995. The authors gratefully acknowledge financial support for this research provided by CICYT (Comisión Interministerial de Ciencia y Tecnología), Spain, under Grants MAT94-120-C03-03 and MAT94-15270-E.

References

1. Hillerborg A.; Modéer, M.; Petersson, P.E. *Cem. Concr. Res.* **1976,** *6,* 773–782.
2. Wittmann, F.H.; Roelfstra, P.E. In *Fracture Toughness and Fracture Energy of Concrete;* Wittmann, F.H., Ed.; Elsevier: Amsterdam, 1986, pp 163–175.
3. Carpinteri, A. In *Static and Dynamic Fracture Mechanics;* Aliabadi, M.H.; et al., Eds.; Computational Mechanics Publications: Southampton, 1994, pp 311–365.
4. Reinhardt, H.W. *Heron* **1984,** *29.*
5. van Mier, J.G.M. In *Applications of Fracture Mechanics to Reinforced Concrete;* Carpinteri, A., Ed.; Elsevier: Amsterdam, 1990, pp 95–135.
6. Barr, B.I.G.; Brokenshire, D.R. In *Fracture Mechanics of Concrete Structures, Vol. 1;* Wittmann, F.H., Ed.; AEDIFICATIO: Freiburg, Germany, 1995, pp 3–16.
7. Elfgren, L. In *Fracture Toughness and Fracture Energy;* Mihashi, H.; et al., Eds.; Balkema: Rotterdam, 1989, pp 575–590.
8. Planas, J.; Elices, M. *Int. J. Fracture* **1991,** *51,* 139–157.
9. Ingraffea, A.R.; Gerstle, W.H. In *Application of Fracture Mechanics to Cementitious Composites;* Shah, S.P., Ed.; Martinus Nijhoff: Dordrecht, The Netherlands, 1985, pp 247–285.
10. Li, V.C.; Chan, C.M.; Leung, C.K.Y. *Cem. Concr. Res.* **1987,** *17,* 441–452.
11. Gerstle, W.H.; Xie, M. *J Eng. Mech.* **1992,** *118,* 416–434.
12. Mihashi, H. In *Fracture Mechanics of Concrete Structures;* Bazant, Z.P., Ed.; Elsevier: London, 1992, pp 239–250.
13. Rokugo, K.; Iwasa, M.; Suzuki, T.; Koyanagi, W. In *Fracture Toughness and Fracture Energy of Concrete;* Wittmann, F.H., Ed.; Elsevier Science: Amsterdam; 1986, pp 163–175.
14. Mai, Y.W. In *Applications of Fracture Mechanics to Reinforced Concrete;* Carpinteri, A., Ed.; Elsevier: New York, 1990, 201–229.
15. Karihaloo, B.L.; Nallathambi, P. *Cem. Concr. Res.* **1989,** *19,* 603–610.
16. Bazant, Z.P., Li, Y.-N. *Appl. Mech. Rev.* **1994,** *47*(6), S91–S96.
17. Dugdale, D.S. *J. Mech. Physics Solids* **1960,** *8,* 100–108.
18. Barenblatt, G.J. *Adv. Appl. Mech.* **1962,** *7,* 55–125.
19. Planas, J.; Elices, M.; Guinea, G.V. *Int. J. Fracture* **1993,** *63,* 173–187.
20. Elices M.; Planas, J. In *Fracture Mechanics of Concrete Structures;* Elfgren, L., Ed.; Chapman & Hall: London, 1989, pp 16–66.
21. Elices, M.; Planas, J.; Guinea, G.V. In *Fracture and Damage of Concrete and Rock;* Rossmanith, H.P., Ed.; E & FN Spon: London, 1993, pp. 3–33.
22. Guinea, G.V.; Planas, J.; Elices, M. In *Size Effect in Concrete Structures;* Mihashi, H.; Okamura, H.; Bazant, Z.P., Eds.; E & FN Spon: London, 1994, pp 233–244.
23. Planas, J.; Guinea, G.V.; Elices, M. In *Fracture Mechanics of Concrete Structures, 1;* Wittmann, F.H., Ed.; AEDIFICATIO: Freiburg, Germany, 1995, pp 95–110.
24. Petersson, P.E. *Crack growth and development of fracture zone in plain concrete and similar materials,* report No. TVBM-1006; Lund Institute of Technology, 1981.
25. Roelfstra, P.E.; Wittman, F.H. In *Fracture Toughness and Fracture Energy of Concrete;* Wittmann, F.H., Ed.; Elsevier Science: Amsterdam, 1986, pp 163–175.
26. Wittmann, F.H.; Roelfstra, P.E.; Mihashi, H.; Huang, Y.Y.; Zhang, X.H.; Nomura, N. *Mater. Struct.* **1987,** *20,* 103–110.
27. Ulfkjaer, J.P.; Brincker, R. In *Fracture and Damage of Concrete and Rock;* Rossmanith, H.P., Ed.; E & FN Spon: London, 1993, pp 135–144.
28. Uchida, Y.; Kurihara, N.; Rokugo, K.; Koyanagi, W. In *Fracture Mechanics of Concrete Structures, 1;* Wittmann, F.H., Ed.; AEDIFICATIO: Freiburg, Germany, 1995, pp 17–30.
29. Guinea, G.V.; Planas, J.; Elices, M. *Mater Struct.* **1994,** *27,* 99–105.
30. RILEM. *Mater. Struct.* **1985,** *18,* 285–290.
31. Guinea, G.V.; Planas, J.; Elices, M. *Mater. Struct.* **1992,** *25,* 212–218.
32. Planas, J.; Elices, M.; Guinea, G.V. *Mater. Struct.* **1992,** *25,* 305–312.
33. Elices, M.; Guinea, G.V.; Planas, J. *Mater. Struct.* **1992,** *25,* 327–334.
34. Planas, J.; Elices, M. In *Fracture Mechanics of Concrete Structures;* Bazant, Z.P., Ed.; Elsevier Applied Science: London, 1992, pp 939–950.
35. Llorca, J.; Planas, J.; Elices, M. In *Fracture of Concrete and Rock;* Shah, S.P.; et al., Ed.; Elsevier Science: Amsterdam, 1989, pp 357–368.
36. Elices, M.; Planas, J. In *Analysis of Concrete Structures by Fracture Mechanics;* Elfgren, L., Ed.; Chapman & Hall: London, 1990, pp 99–127.
37. Planas, J.; Elices, M. *Int. J. Fracture* **1992,** *55,* 153–177.
38. Planas, J.; Elices, M. *Int. J. Fracture* **1993,** *64,* 221–237.
39. Elices, M.; Planas, J. *Int. J. Fracture* **1993,** *61,* 259–272.
40. Planas, J.; Elices, M.; Ruiz, G. *Int. J. Fracture* **1993,** *61,* 231–246.
41. Bazant, Z.P.; Kim, J.K.; Pfeiffer, P.A. *J. Struct. Engin.* **1986,** *112,* 289–307.
42. Bazant, Z.P.; Kazemi, M.T. *Int. J. Fracture* **1990,** *44,* 111–131.
43. Jenq, Y.S.; Shah, S.P. *J. Eng. Mech. Div.* **1985,** *111,* 1227–1241.
44. Ouyang, C.; Mobasher, B.; Shah, S.P. *Eng. Fracture Mech.* **1990,** *37,* 901–913.
45. Ouyang, C.; Shah, S.P. *J. Am. Ceram. Soc.* **1991,** *74,* 2831–2836.
46. Planas, J.; Elices, M.; Toribio, J. In *Fracture of Concrete and Rock;* Shah, S.P.; et al., Eds.; Elsevier Science: Amsterdam, 1989, pp 203–212.
47. RILEM. *Mater. Struct.* **1990,** *23,* 461–465.
48. RILEM. *Mater. Struct.* **1990,** *23,* 457–460.
49. Elices, M.; Planas, J. In *Applications of Fracture Mechanics to Reinforced Concrete;* Carpinteri, A.; Ed.; Elsevier: Amsterdam, 1992, pp 169–200.
50. Planas, J.; Elices, M. *Eng. Fracture Mech.* **1990,** *35,* 87–94.